Research Square

Preprints are preliminary reports that have not undergone peer review.
They should not be considered conclusive, used to inform clinical practice,
or referenced by the media as validated information.

Study on helical hole-making process of CFRP/Al alloy laminated materials

Xue Li (2697068527@qq.com)
University of Science and Technology Liaoning
Anyuan Jiao
University of Science and Technology Liaoning https://orcid.org/0000-0003-3606-5589
Binghong Liu
Yue Zhang
Guojun Liu
Zhen Zhang

Research Article

Keywords: Helical milling, Response surface method (RSM), Variable parameters, Micro-lifting tool

Posted Date: March 18th, 2022

DOI: https://doi.org/10.21203/rs.3.rs-1448221/v1

License: This work is licensed under a Creative Commons Attribution 4.0 International License.
Read Full License

Abstract

To ensure assembly accuracy and efficiency, lots of holes are made directly on the laminated material composed of CFRP and Al alloys. However, because the different laminated sequence, the optimal process parameters are also different, which affects the hole-making quality of the laminated materials. First, the motion of helical milling was analyzed. Level values of influence the quality of the hole-making are determined, such as spindle speed, pitch and preload. The response surface method (RSM) was used to design experiments, and the burr height between Al alloy interlayer and the tear value of CFRP were used as the standard to analyze the experimental results. The optimal parameters combination for different laminated sequences were predicted and used for cutting force analysis. Secondly, the hole-making processes with variable parameters study were carried out, and the method of micro-lifting tool is proposed for the experimental study of the sudden change of axial force in the transition between interlayer with constant parameters. The results show that the aperture of the hole-making with variable parameters of the laminated materials using the optimal process parameters all meets the H9. The interlayer burr of the Al alloy and the tear value of the CFRP at the entrance and exit conform to the technical requirements. The hole-making axial forces of the laminated material are less than 50 N and 60 N, which are 70% and 83% of constant parameters milling. The effectively reduce the sudden change of axial force between interlayer.

1 Introduction

CFRP has been widely used as a structural part or functional part in aerospace and other fields due to their low density, high specific modulus, high specific strength, strong corrosion resistance, high temperature resistance and other excellent properties [1–5]. Aluminum alloy is one of the commonly used metal materials in aircraft structures due to their low density, corrosion resistance, high fatigue resistance and high specific strength [6–7]. Advanced composite materials, aluminum alloys and titanium alloys are the most widely used laminated materials in the aerospace field [8]. However, the laminated structure of CFRP and Al alloy occupies a very large proportion in aircraft structural parts [9]. But integrated hole-making of two or more aerospace materials has always been a challenge in aerospace manufacturing, especially for laminations between different materials [10].

In recent years, scholars at home and abroad have carried out a lot of study on the hole-making of laminated materials [11]. Liang [12] and Li et al. [13] conducted drilling experiments on metal laminated materials, and the size of the interlayer gap has a significant influence on the size of the interlayer burr. Luo et al. [14] proposed an optimization method for the preparation process of assembly components of laminated materials and technical scheme for hole-making by step combination. This study has greatly improved the quality of the hole-making in laminated materials. The aperture accuracy of the laminated structure is one of the important factors to affect the fatigue performance of the connector [15]. Zitoune et al. [16] conducted drilling experiments on CFRP/Al alloy laminations. The results show that the phenomenon of shrinkage holes occurs when the CFRP aperture is smaller than the drill bit diameter. However, Li et al. [17] found that there is still room for improvement in the current drilling process, and the

problem of shrinkage holes in laminated materials is effectively avoided. Zhang et al. [18] conducted experimental study on the drilling of carbon fiber composites/titanium alloy laminations, and proposed a method of changing process parameters in the transition area of the laminations. Wang et al. [19] conducted an experimental study on the drilling of CFRP/Al laminations. The influence of different laminated sequences on the axial force was studied. The results show that the hole-making quality is significantly improved when drilling from the side of the two materials. Sun et al. [20] measured the axial force of hole-making in the CFRP/ aluminum alloy laminated drilling experiment, and discussed the influence of spindle speed and feed rate on the axial force of laminated hole-making. Wang et al. [21] designed an experiment for drilling CFRP/titanium alloy laminations based on chip breaking process method. The results show that this can effectively improve the hole wall surface quality of CFRP and titanium alloys. Wei [22] studied the CFRP/aluminum alloy laminations, analyzed the process problems in the hole-making process with constant parameters, and proposed a process method of hole-making with variable parameters. Wang et al. [23] proposed a method of setting feed rate based on geometric function to reduce fiber tear and burr height caused by CFRP/Al laminated hole-making.

As a new type of hole machining technology, helical milling realizes hole machining by the revolving movement of the tool around the hole axis while the tool rotates around the tool axis [24–25]. Compared with the traditional drilling process, helical milling adopts eccentric machining, which eliminates the Influence of the traditional twist drill chisel edge, reduces the axial force and greatly improves the machining quality [26–27]. Ni et al. [28] first proposed the concept of helical milling technology for machining CFRP/Ti laminations. Shan [29] used CFRP/light alloy laminated materials to conduct experimental study, and theoretical analysis, numerical simulation and cutting experiments are used. The study focuses on the basic process of helical milling, milling force, process optimization and other aspects. Wang et al. [30] studied the machining dynamics of helical milling of titanium alloy/carbon fiber laminated materials, and found that helical milling can reduce burr sizes of metals and reduce delamination of carbon fiber reinforced plastics. Lei Sun et al. [31] used two methods of drilling and helical milling to study the damage generation mechanism of titanium/CFRP/aluminum laminations. Based on the orthogonal experimental method, the main reasons for the damage in the process of machining are studied. Huang et al. [32] carried out an experimental study on helical milling of CFRP/titanium alloy laminations by using parameters decreasing variation and reciprocating variation processing. The experiments were carried out to analyze the surface roughness of the hole wall and the hole error.

In summary, drilling technology in laminated materials has matured, and helical milling has been used to study holes in laminated materials. With the further improvement of the machining requirements of laminated materials, the constant parameters cannot meet the quality requirements, and the experimental and theoretical analysis of laminated materials needs to be further improved. This paper aims to improve the quality and efficiency of hole-making. First, based on the RSM, experiments were designed to analyze the influence of spindle speed, pitch and preload on hole-making. According to the prediction results, the optimal parameters combination of CFRP and Al alloy were obtained. Secondly, hole-making processes with variable parameters study were carried out based on the optimal parameters combination for hole-

making, and micro-lifting tool method was proposed for the sudden change of axial force between interlayers with constant parameters. This will improve the quality of the hole-making.

2 Motion Analysis Of Helical Milling

Helical milling hole usually uses a tool to complete a variety of holes greater than or equal to the tool diameters. The principle of hole- making is shown in Fig. 1. The movement process can be decomposed into two kinds of movement that one is the feed motion of the tool in the circumferential direction and the other is the feed motion of the tool in the axial direction.

The eccentric amount of axis during revolution motion and rotation motion in the process of helical milling is ignored. The angle relationship can be shown in Fig. 2.

As shown in Fig. 2, the coordinate of any point *P* on the tool at time *t* is:

$$\begin{cases} x(t) = r_0 \cdot \cos\beta + r_s \cdot \cos\alpha \\ y(t) = r_0 \cdot \sin\beta + r_s \cdot \sin\alpha \\ z = -ft = h_0 \end{cases}$$

1

In the Eq.: time-t; theoretical revolution radius-r_0; theoretical tool radius-r_s; axial initial coordinate value-h_0; axial feed rate-f.

When $t = 0$, the revolution angle $\beta = 0$, the rotation angle α is equal to the initial angle α_0. When the rotation speed is n, the revolution speed is n_p, then:

$$\begin{cases} \alpha = \alpha_0 + \dfrac{2\pi n_p}{60} t \\ \beta = \dfrac{2\pi n}{60} t \end{cases}$$

2

According to Eq. (1) and Eq. (2):

$$\begin{cases} x(t) = r_0 \cdot \cos\dfrac{2\pi nt}{60} + r_s \cdot \cos\left(\alpha_0 + \dfrac{2\pi n_p}{60}t\right) \\ y(t) = r_0 \cdot \sin\dfrac{2\pi nt}{60} + r_s \cdot \sin\left(\alpha_0 + \dfrac{2\pi n_p}{60}t\right) \\ z = -ft = h_0 \end{cases}$$

3

If the column matrix is $S = [t, r_0, r_s, \alpha_0, h_0, n, n_p, f]^T$, it can be seen that the matrix S determines the P point.

The Python software is used to import the motion equation and input the corresponding parameters of matrix S, which can generate the trajectory of the tool nose, end edge and side edge.

When using φ5 mm tool to mill φ6 mm hole, the corresponding parameters are: r_0 = 0.5 mm, R_t = 2.5 mm, n = 3000 r/min, n_p=120 r/min, α_0 = 0, f = 0.15 mm/s. The trajectory equation and simulation results are:

(1) tool nose

Since the tool nose satisfies $r_s = D_t/2 = R_t$, $h_0 = 0$, the Eq. (4) is simplified by substituting they into the equation.

$$\begin{cases} x(t) = r_0 \cdot \cos\dfrac{2\pi nt}{30} + R_t \cdot \cos\left(\alpha_0 + \dfrac{2\pi n_p}{30}t\right) \\ y(t) = r_0 \cdot \sin\dfrac{2\pi nt}{30} + R_t \cdot \sin\left(\alpha_0 + \dfrac{2\pi n_p}{30}t\right) \\ z = -ft \end{cases}$$

4

In a four-blade tool, the trajectory curve of one tool nose from t = 0 to t = 1s is as follows:

It can be seen from the figure that the tool nose revolves around the axis of the hole while rotating around the axis of the milling tool.

(2) end edge

The end edge can be regarded as a collection of a series of points, and satisfies $0 \leq r_s \leq R_t$, $h_0 = 0$. Its equation satisfies:

$$x(t) = r_0 \cdot \cos\frac{\pi nt}{30} + r_s \cdot \cos\left(\alpha_0 + \frac{\pi n_p}{30}t\right)$$

$$y(t) = r_0 \cdot \sin\frac{2\pi nt}{30} + r_s \cdot \sin\left(\alpha_0 + \frac{\pi n_p}{30}t\right)$$

$$z = -ft$$

$$0 \leqslant$$

{
5

In a four-blade tool, the trajectory curve of one end edge from $t = 0$ to $t = 1$s is shown in Fig. 4. It can be seen that during the helical milling process, the cutting trajectory of the end edge is a continuous helical curved surface.

(3) side edge

The side edge can also be regarded as a collection of a series of points, and satisfies $-ft \leq h_0 \leq 0$, rs = Rt, and its equation satisfies:

\left\{ \begin{gathered} x(t)={r_0} \cdot \cos \frac{{\pi nt}}{{30}}+{R_t} \cdot \cos \left({{\alpha _0}+\frac{{\pi {n_p}}}{{30}}t} \right) \\ y(t)={r_0} \cdot \sin \frac{{2\pi nt}}{{30}}+{R_t} \cdot \sin \left({{\alpha _0}+\frac{{\pi {n_p}}}{{30}}t} \right) \\ z= - ft+{h_0} \\ - ft \leqslant h0 \leqslant 0 \\ \end{gathered} \right.
6

In a four-blade tool, the trajectory curve of one side edge from $t = 0$ to $t = 1$s is shown in Fig. 5. It can be seen that different from the cutting of end edge, the side edge trajectory is not circular. And one week per revolution, the side edge is not in contact with the hole wall for some time. Therefore, the cutting of each side edge is discontinuous.

3 The Experiment Of Helical Milling

3.1 Experimental conditions

The material used in this experiment are 2024 Al alloy and CFRP, and the fiber type of CFRP is T700. Al alloy with a size of 150 mm×100 mm×2 mm and CFRP with a size of 150 mm×95 mm×5 mm are selected as shown in Fig. 6. The material of the four-edge milling tool is cemented carbide (tungsten steel) and the diameter is 5 mm. The diameter of the hole is 6 mm. The basic parameters of the milling tool are shown in Table 1.

Table 1
Tool parameters

Overall length (mm)	Blade length (mm)	HRC	Helical angle (°)
20	15	58	35

3.2 Experimental design

According to literature [33,34], it can be seen that the most important factors of influence the quality of hole-making are spindle speed and pitch. Secondly, some studies have found that hole-making of applying preload has significant inhibitory effect on the burr height and damage of the interlayer gap. This is because the formation of burrs between laminations is inhibited by inhibiting the extra gap under the action of flow force when hole-making of applying preload [35]. Therefore, this paper chooses the preload as the third influence factors for the helical milling of laminated materials. Through experiments, it is found that when the spindle speed is between 2000 r/min and 3000 r/min, the pitch is between 1.5 mm and 2.2 mm, which has greater impact on the quality of the hole.Therefore, the selected factor levels are shown in Table 2.

Table 2
Factor level table

Level	Spindle speed-*A* (rpm)	Pitch-*B* (mm)	Preload-*C* (N)
1	2000	0.1	240
2	3000	0.2	360
3	4000	0.3	480

3.3 Analysis of Al alloy/CFRP

Taking spindle speed, pitch and preload as design variables and taking exit burrs of Al alloy and damage values of CFRP as response values. The 17 groups of response surface experiments were obtained by BBD experimental design as shown in Table 3.

Table 3 Experimental results

No.	Spindle speed-*A* (rpm)	Pitch-*B* (mm)	Preload-*C* (N)	Results (mm)
1	3000	0.3	240	44.2 0.59 0.545 40.6
2	3000	0.2	360	16.2 0.41 0.19 11.7
3	3000	0.1	480	27.2 0.16 0.11 24.2
4	2000	0.2	240	44.8 0.855 0.415 36.9
5	3000	0.1	240	32.5 0.23 0.15 28.9
6	3000	0.2	360	16.2 0.42 0.19 12
7	4000	0.2	480	38.6 0.13 0.13 32.5
8	3000	0.2	360	17.8 0.415 0.195 11.5
9	2000	0.2	480	38.2 0.79 0.455 35.4
10	2000	0.3	360	48.5 1.25 0.875 45.2
11	3000	0.2	360	15.6 0.415 0.195 12.2
12	3000	0.3	480	34.3 0.52 0.39 38.4
13	2000	0.1	360	39.8 0.71 0.21 31
14	4000	0.3	360	43.5 0.44 0.29 38.9
15	3000	0.2	360	15.8 0.4 0.185 12.5
16	3000	0.2	240	41.5 0.31 0.16 36.1
17	4000	0.1	360	42.0 0.12 0.065 32.4

The maximum burr for the Al alloy at the entrance and exit are listed in Table 3 respectively. Through the nonlinear fitting method, the variables and the size of the burr at the entrance and exit of the Al alloy are subjected to multiple regression fitting and the following mathematical model of the multiple regression equation is obtained. Where A-spindle; B-pitch; C-preload.

$$\begin{gathered} H=273 - 0.09995A - 293.35B - 0.4185C - 0.018AB \hfill \\ {\text{+}}7.708 \times {10^{ - 6}}AC - 0.0958BC+1.6677 \times {10^{ - 5}}{A^2} \hfill \\ +1045.25{B^2}+5.401 \times {10^{ - 4}}{C^2} \hfill \\ \end{gathered}$$

7

After the mathematical model of the regression equation is obtained, it is necessary to further test the fit and reliability of the model itself. The regression equation analysis of variance table is obtained as shown in Table 4.

It can be seen from Table 4that the F value is 108.95 and the Prob > F value is 0.0001. It is less than 0.05 that the model is significant, which means that the regression equation is valid and the significance is very high. The Prob > F value of lack of fit of the model is 0.0597 greater than 0.05. This indicates that it is not significant. It can be seen from the table that the Prob > F values of B and C are far less than 0.05, which indicates that their influence on hole-making is relatively large.

Table 4
Variance analysis

Source of variance	Sum of square	F	Prob > F
Model	2285.37	108.95	< 0.0001
A	4.06	1.74	0.2284
B	105.13	45.10	0.0003
C	76.26	32.72	0.0007
AB	12.96	5.56	0.0505
AC	3.42	1.47	0.2649
BC	5.29	2.27	0.1757
A^2	1171.11	502.45	< 0.0001
B^2	460.02	197.37	< 0.0001
C^2	254.69	109.27	< 0.0001
Residual	16.32		
Lack of fit	13.31	5.90	0.0597

It can be seen from Fig. 7(a) that the residual arrangement is approximately a straight line. It can be seen from Fig. 7(b) that each experimental point is relative dispersed. All these indicate that the model has high concordance between the prediction value of the burr height of the Al alloy and the experimental value.

The RSM is used to analyze the results and while one experimental factor remains unchanged, the influence of the interaction between other experimental factors on the burr height of the Al alloy at the entrance and exit are explored.

It can be seen from Fig. 8(a) that when the preload remains constant, with the increase of the spindle speed, the Al alloy burr height first decreases and then increases. When the spindle speed is about 3000 r/min, the burr height increases. The value tends to be stable and the burr height decreases to the lowest value when the pitch is about 0.18 mm.

It can be seen from Fig. 8(b) that when the pitch remains constant, the burr height first decreases and then increases with the increase of the spindle speed and the overall change trend is obvious. When the spindle speed is around 3000 r/min, the burr height trend to be stable. And the burr height first decreases and then tends to be stable with the increase of preload, but the overall change trend is not obvious. When the spindle speed is around 3000 r/min and the preload is around 380 N, the burr height is reduced to the lowest level.

It can be seen from Fig. 8(c) that when the spindle speed remains constant, the burr height first decreases with the increase of the pitch, tends to be stable and then increases greatly. This shows that the burr height trend to be stable when the pitch is in the range of 0.1–0.2 mm. However, the efficiency of hole-making is considered. The pitch is 0.2 mm. And the burr height first decreases and then tends to be stable with the increase of the preload. When the preload reaches about 380 N, the burr reaches the lowest level and tend to be stable state.

The RSM is used to predict the experimental results of Al alloy, with the minimum burr height at the exit as the goal, the optimal parameters combination is obtained as shown in Fig. 9.

For CFRP, the maximum tear value at the entrance and exit is used as the criterion for analysis. Therefore, the tear value of CFRP are listed in Table 3.

The multiple regression fitting is performed on the variables and the exit tear value of CFRP by the nonlinear fitting method, and the following the multiple regression equation is obtained. Table 5 is the regression equation of variance analysis table.

$$\begin{gathered} H=1.81875 - 1.2708 \times {10^{ - 3}}A - 2.34B+3.5552 \times {10^{ - 3}}C \hfill \\ - 5.5 \times {10^{ - 4}}AB - 1.7708 \times {10^{ - 7}}AC+2.632 \times {10^{ - 17}}BC \hfill \\ +1.85875 \times {10^{ - 7}}{A^2}+3.2125{B^2} - 4.80035 \times {10^{ - 6}}{C^2} \hfill \\ \end{gathered} \tag{8}$$

Table 5
Variance analysis

Source of variance	Sum of square	F	Prob > F
Model	1.38	128.56	< 0.0001
A	0.87	726.60	< 0.0001
B	0.31	261.25	< 0.0001
C	0.022	18.02	0.0038
AB	0.012	10.13	0.0154
AC	1.806E-003	1.51	0.2585
BC	0.000	0.000	< 0.0001
A^2	0.15	121.79	< 0.0001
B^2	4.345E-003	3.64	0.0981
C^2	0.020	16.84	0.0045
Residual	1.194E-003		
Lack of fit	2.710E-003	27.14	0.054

The F is used to judge the significant degree of each item. A large F value and small Prob > F value represent higher significance of the relevant items [36]. The F value is 128.56 and the Prob > F value is less than 0.0001. Pitch and the interaction of pitch and preload have very significant influence on the tear. Therefore, within the parameter range selected in the experiment, the sequence of influence degree on the response value are pitch > spindle speed > preload.

The distribution of experimental data in Fig. 10(a) is approximately a straight line, and the experimental points in Fig. 10(b) are also relative dispersed. In general, this model is reliable for predicting the tear value of CFRP holes.

The RSM is used to analyze the results, and while one experimental factor remains unchanged, the influence of the interaction between other experimental factors on the burr height of the Al alloy at the entrance and exit is explored.

It can be seen from Fig. 11(a) that when the preload remains constant, with the increase of the spindle speed, the tear value of the CFRP at the entrance first decreases and then remains stable. At about 3000 r/min of spindle speed, the tear value of CFRP tends to be stable. When the spindle speed is about 3500 r/min and the pitch is about 0.11 mm, the burr height is reduced to the lowest.

It can be seen from Fig. 11(b) that the interaction between the spindle speed and the preload is not significant. When the pitch remains constant, the tear value of the CFRP at the entrance and exit decreases first and then tends to be stable with the increase of the spindle speed, and the overall change trend is not obvious. When the spindle speed is around 3600 r/min, the tear value began to stabilize. And the tear value decreases first and then tends to be stable with the increase of the preload, but the overall change trend is obvious. When the spindle speed is about 3600 r/min and the preload is about 430 N, the tear value of the hole edge is reduced to the lowest.

It can be seen from Fig. 11(c) that when the spindle speed remains constant, the burr height first increases slightly and then greatly increases with the increase of the pitch, which shows that when the pitch is in the range of 0.1–0.13 mm, the tear value along the hole tends to be stable. When the spindle speed remains constant, the burr height decreases first and then tends to be stable with the increase of the preload. When the preload reaches about 450 N, the tear value along the hole reaches the minimum and tends to be stable state.

The RSM is used to predict the experimental results of CFRP, with the minimum tear value at the exit as the goal, the optimal process parameters combination is obtained as shown in Fig. 12.

3.4 Analysis of CFRP/ Al Alloy

Similar to the analysis of the measurement results of the laminated materials, the tear value of the CFRP material and the maximum burr at the entrance and exit of the Al alloy are also used as the response value. And the 17 groups of response surface experiments are obtained by the BBD experimental design. The tear value for the CFRP at the entrance and exit are listed in Table 3, and the following mathematical model of multiple regression equation is obtained. Table 6 is the regression equation of variance analysis.

$$\begin{gathered} H=0.61687 - 3.72 \times {10^{ - 4}}N - 2.56375{a_p} - 2.1979 \times {10^{ - 4}}F \hfill \\ - 1.1 \times {10^{ - 3}}N{a_p} - 1.45833 \times {10^{ - 5}}NF - 2.39588 \times {10^{ - 3}}{a_p}F \hfill \\ +8.0123 \times {10^{ - 8}}{N^2}+8.8875a_{p}^{2}+1.31076 \times {10^{ - 6}}{F^2} \hfill \\ \end{gathered} \quad (9)$$

It can be seen from Table 6 that the F value is 36.05, and the Prob > F value is less 0.0001. It less than 0.05 indicates that the model term is significant. At the same time, the interaction between the pitch and the spindle speed also has very significant influence on the tear value. Within the range of parameters selected in the experiment, the significant degree of their influence on the response value are pitch > spindle speed > preload.

Table 6
Variance analysis

Source of variance	Sum of square	F	Prob > F
Model	0.64	36.05	< 0.0001
A	0.21	107.2	< 0.0001
B	0.31	154.03	< 0.0001
C	4.28E-003	2.15	0.1858
AB	0.048	24.35	0.0017
AC	1.225E-003	0.62	0.4582
BC	3.306E-003	1.66	0.2381
A^2	0.027	13.60	0.0078
B^2	0.033	16.73	0.0046
C^2	1.500E-003	0.75	0.4138
Residual	1.988E-003		
Lack of fit	0.060	7.08	0.0445

The distribution of experimental data in Fig. 13 (a) approximates a straight line. Each experimental point in Fig. 13(b) is also relative dispersed. In general, this model is reliable for the predicting the tear value of CFRP holes.

It can be seen from Fig. 14(a) that when the preload remains constant, with the increase of the spindle speed, the tear value at the entrance and exit has decreasing trend. When the spindle speed is about 3600 r/min, the tear value reaches the minimum and when the pitch is about 0.1 mm, the tear value is reduced to the minimum.

It can be seen from Fig. 14(b) that when the pitch remains constant, the tear value at the entrance and exit decreases with the increase of the spindle speed. When the spindle speed is around 3600 r/min, the tear value tends to be stable. When the pitch remains constant, the tear value along the hole slowly decreases with the increase of the preload and then tends to be stable, but the decreasing trend is slow. When the spindle speed is around 3700 r/min and the preload is around 460 N, the tear value is reduced to the minimum.

It can be seen from Fig. 14(c) that when the spindle speed remains constant, the tear value at the entrance and exit decreases with the decrease of the pitch, but the influence of preload on the tear value is not obvious, and the trend of change is also slow.

The RSM is used to predict the experimental results of CFRP, with the minimum tear value at the exit as the goal, the optimal process parameters combination is obtained as shown in Fig. 15.

Similarly, the measured burr height for the Al alloy at the entrance and exit are listed in Table 3, and the following multiple regression equation is obtained. Table 7 is the regression equation of variance analysis table.

$$\begin{gathered} H=250.125 - 0.076935A - 356.65B - 0.49467C \hfill \\ - 0.01925AB - 4.375 \times {10^{ - 6}}AC+0.052083BC \hfill \\ +{1.3547510^{ - 5}}{A^2}+1134.75{B^2}+6.73437 \times {10^{ - 4}}{C^2} \hfill \\ \end{gathered}$$
9

Table 7
Variance analysis

Source of variance	Sum of square	F	Prob > F
Model	2223.11	376.46	< 0.0001
A	9.25	14.09	0.0071
B	271.45	413.70	< 0.0001
C	18.00	27.43	0.0021
AB	14.82	22.59	0.0021
AC	1.10	1.68	0.2360
BC	1.56	2.38	0.1667
A^2	772.78	1177.76	< 0.0001
B^2	542.17	826.30	< 0.0001
C^2	395.96	603.47	< 0.0001
Residual	1.988E-003		
Lack of fit	0.060	7.08	0.0445

It can be seen from Table 7 that the F value is 376.46, and the model Prob > F value is less than 0.0001. If it is less than 0.05, the model is significant. The pitch and the interaction between the pitch and the spindle speed also have very significant influence on the tear.

The distribution of experimental data in Fig. 16(a) approximates a straight line. The experimental points in Fig. 16(b) are also relative dispersed. In general, this model is reliable for the predicting the burr height.

It can be seen from Fig. 17(a) that when the preload remains constant, with the increase of the spindle speed, the burr height of the Al alloy at the exit first decreases and then increases, and when the spindle

speed is about 3000 r/min, the burr height tends to be stable. When the spindle speed is about 3500 r/min, the burr height begins to rise. When the pitch is between 0.15 mm and 0.22 mm, the burr height tends to be stable.

It can be seen from Fig. 17(b) that when the preload remains constant, the burr height first decreases and then increases with the increase of the spindle speed. The influence is very small. When the spindle speed is around 2900 r/min, the burr height begins to be stable. Under the condition that the pitch remains constant, the burr height only increases slightly with the increase of the preload, but the overall change is not obvious. When the spindle speed is around 2900 r/min and the preload is around 360 N, the burr height is reduced to the lowest level.

It can be seen from Fig. 17(c) that when the spindle speed remains constant, the burr height first decreases with the increase of the pitch, tends to be stable and then increases greatly, which indicates that the size of the pitch should be 0.16–0.21 mm range to choose.

Based on the analysis of these four groups, it can be seen that the factors of influence the quality of hole-making are pitch > spindle speed > preload. However, the preload has great influence on the quality of the interlayer gap of the hole-making materials.

The RSM is used to predict the experimental results of Al alloy, with the minimum burr height at the exit as the goal, the optimal parameters combination is obtained as shown in Fig. 18.

Taking into account the hole-making efficiency and hole-making quality, the optimal parameters combination for the Al alloy are obtained: the spindle speed is 3000 r/min, the pitch is 0.17 mm, and the preload is 380 N. The optimal parameters combination of CFRP are obtained: the spindle speed is 3700 r/min, the pitch is 0.11 mm, and the preload is 430 N.

3.5 Analysis of cutting force

In the machining process, important physical quantities such as the cutting state of the material, cutting quality and tool life can be reflected by cutting force and axial force. Therefore, it is of great significance to study the cutting force and axial force in the cutting process.

The radial force in the hole-making process is composed of the combined force of the FC3D 120 three-dimensional force sensor in the X direction and the Y direction. The axial force is composed of the force in the Z direction of the sensor. The USB3200 signal collector is mainly used to process the collected signal information and convert it into a signal that can be recognized by the computer. The function of the computer monitor is to display the collected signal visually. The data collection for the force is shown in Fig. 19.

Figures 20(a) and 20(b) are the comparative analysis diagrams of the X and Y direction force and the axial force of the helical milling hole. The axial force during the hole-making process of the laminated materials can be roughly divided into five stages. The first stage is the entrance stage of milling CFRP.

The second stage is the stable milling CFRP. The third stage is the transition stage of milling CFRP/Al alloy laminations. The fourth stage is stable milling Al alloy. The fifth stage is the milling Al alloy exit stage.
Figures 20(a) and 20(b) are machined with the optimal parameters combination of CFRP and Al alloy respectively. Compared with Fig. 20(a), the axial force of CFRP in Fig. 20(b) is about 12 N larger (The axial force are about 39 N and about 50 N respectively), the fluctuation is greater, and the quality of the obtained hole wall is poor. Therefore, the process parameters are not suitable for milling holes of CFRP. On the other hand, although the axial force of Al alloy is 11N in Fig. 20(b) greater than Fig. 20(a) (The axial force are about 41 N and about 52 N respectively), but the fluctuation is small and the efficiency is high. Therefore, this parameters are suitable for milling holes of Al alloy. Although the axial force using the process parameters of Fig. 20(a) is relatively small, it is suitable for CFRP and Al alloy. But because of the low efficiency of this parameters, and the axial force will increase sharply when the milling tool transitions from CFRP to Al alloy. Therefore, hole-making with variable parameters is considered to observe whether this sudden change in force can be eliminated.

4 Experimental Of Hole-making With Variable Parameters

Two groups of optimal process parameters obtained using RSM. They carried out hole-making with variable parameters on four different types of laminated materials of CFRP/Al alloy, Al alloy/CFRP, CFRP/Al alloy/ CFRP, and Al alloy/CFRP/Al alloy. The process parameters used as follows: the spindle speed is 3000 r/min and the pitch is 0.17 mm for the Al alloy hole, the spindle speed is 3700 r/min and pitch is 0.11 mm for the CFRP hole and the preload of the whole hole-making process is 430 N, and the feasibility of hole-making with variable parameters is discussed. Finally, it is analyzed whether the process parameters are suitable for the hole-making with variable parameters of three or more laminated materials.

When experimenting with CFRP/Al alloy laminated materials, the Al alloy is machined first, and the depth is 2 mm. Then the CFRP is machined with variable parameters, and the depth is 5 mm. In the same way, the same method is used for the other three laminated materials.

4.1 Analysis of entrance and exit morphology

In order to meet the precision requirements of hole-making, the morphology of the CFRP hole and the entrance and exit burrs of the Al alloy hole are tested. The influence of the CFRP at the entrance and exit morphology of the hole-making with variable parameters is analyzed and the influence on the burr of the Al alloy at the entrance and exit.

The machining of Al alloy holes requires small burrs at the entrance and exit, and fewer burrs and tears at the entrance and exit of the CFRP hole. This is the evaluation standard to judge the quality of the machining hole.

Using the camera take a picture of the overall morphology of the hole, the maximum tear value in CAD marked, and find the maximum tear value w, as shown in Fig. 21.

It can be seen from Fig. 21 that when using four different laminated materials of hole-making with variable parameters, the maximum tear value of CFRP are 0.2 mm, 0.09 mm, 0.07 mm, 0.12 mm, 0.145 mm. This is far less than the 2.54 mm required for hole-making.

Using a super-depth of field three-dimensional microscope to detect the burr height at the entrance and exit of the Al alloy hole, and the data is shown in Fig. 22.

It can be seen from Fig. 22 that the largest burrs at the entrance and exit of the Al alloy are 4.1μm, 5.4 μm, 5.4 μm, 8.1 μm, and 5.4 μm respectively. The burr height is very small. The results prove that this parameters is suitable for machining Al alloy holes.

4.2 Analysis of aperture and hole wall

The aperture of Al alloy holes and CFRP holes were measured using the claw inner diameter micrometer. Each hole was measured three times, and the average value was finally taken, as shown in Table 8.

Analyzing Table 8 found that the aperture is all within the required range (0 ~ + 43 μm), and the aperture deviation meets the requirements of H9. The aperture will gradually decrease with the cutting depth of the tool. This is due to the gradually weakened of the rigidity of the tool.

Detection of hole wall morphology of Al alloy and CFRP holes by ultra-depth three- dimensional microscope. It can be seen from Fig. 23 that the inner wall of the CFRP hole in the four groups of experiments has clear milling texture and smooth inner wall curve, which shows that the hole-making with variable parameters has significant influence on CFRP. It can be seen from Fig. 24 that the inner wall morphology of the Al alloy holes in the four groups of tests is clear and has no obvious defects. The black materials in the figure is caused by the cutting chips powder after the CFRP hole-making.

Table 8
Aperture value

Layers Name	**1**	**2**	**3**
CFRP/Al alloy	6.025	6.031	
Al alloy/CFRP	6.038	6.009	
CFRP/Al alloy/CFRP	6.025	6.019	6.002
Al alloy/CFRP/ Al alloy	6.036	6.021	6.015

5.3 Analysis of cutting force

When constant parameters are used for hole- making, the axial force in the transition phase will suddenly increase. In the hole-making with variable parameters, the method of micro-lifting the tool is used to eliminate the influence of the elastic deformation of the material on the axial force of hole-making. The sudden increase of the axial force is avoided.

In the hole-making with variable parameters experiment, the cutting force and axial force of the hole-making are roughly divided into two categories. The first category is the cutting force and axial force of the two laminated methods of CFRP/Al alloy and Al alloy/ CFRP. They are roughly divided into five stages. The details are shown in Fig. 25 and Fig. 26.

It can be seen from Fig. 25(a) that in the first stage, when the tool just contacts the CFRP, the axial force increased sharply from 0 N to about 48 N in short time, and there are large fluctuations. This is due to the instability caused by the tool spiraling in contact with the material. The duration of this fluctuation is about the time of one revolution of the tool. After entering the second stage, the tool is completely milled into the CFRP. At this time, the axial force curve fluctuates slightly, and the fluctuation value is between 30 N and 35 N. The reason for the fluctuation is that the contact between the tool and the workpiece is discontinuous during the milling process because the nonlinearity of the CFRP material. But the fluctuations at this stage are stable within a certain range, and there are obvious stable characteristics. However, the Al alloy has better continuity, so the axial force fluctuation is better than the CFRP. The third stage is that the milling tool enters the Al alloy from the CFRP, and this stage is also the parameters change stage. The change process is accompanied by the action of to eliminate the sudden increase in the axial force caused by the elastic deformation of the material. When the tool first contacts the Al alloy, the axial force increases sharply from 0 N to about 50 N in short time, and then tends to a stable state. The stability of the axial force when milling Al alloys is better than the CFRP. The fourth stage is similar to the second stage, it belongs to the stable milling stage, the axial force of this stage is about 50 N. The fifth stage is that the milling tool is about to complete the Al alloy machining. In this stage, the milling axial force is gradually reduced from 50 N to 0 N. The bottom edge of the tool is milled out of the material until it completely penetrates the material, and the side edge of the tool continues to complete the hole-making process. The duration of this stage is longer than the ideal state. The main reason is that the uncut parts of Al alloy and CFRP will produce elastic deformation. And the elastic deformation will increase with the reduction of uncut parts of Al alloy until the hole-making machining is completed. Milling of the Al alloy/CFRP laminations as shown in Fig. 25(b) also goes through the above five stages.

The second category is the cutting force and axial force of the two laminated methods of CFRP/Al alloy/CFRP and Al alloy/CFRP/Al alloy. Because these two laminated materials are composed of three layers materials, there are two transition stages, so it can be roughly divided into seven stages. Take CFRP/Al alloy/CFRP laminated materials as an example.

It can be seen from Fig. 26(a) that in the first stage, when the tool just contacts the CFRP, the axial force increased sharply from 0 N to about 25 N in short time, and there are big fluctuation. But it will soon enter the second stage. The tool is completely milled into the CFRP. At this time, the axial force fluctuates

slightly between 20 N and 25 N. But the fluctuations in this stage are stable within a certain range. The Al alloy has better continuity, so the axial force fluctuation is better than the CFRP. The third stage is that the milling tool enters the Al alloy from the CFRP, and this stage is also the parameters change stage. The change process is accompanied by the action of micro-lifting tool to eliminate the sudden increase in the axial force. When the tool first contacts the Al alloy, the axial force increases sharply from 0 to about 50 N in short time, and then tends to a stable state. The stability of the axial force when milling Al alloy is better than the CFRP. The fourth stage is similar to the second stage, it belongs to the stable milling stage, the axial force of this stage is about 50 N. The fifth stage is the transition stage from Al alloy to CFRP material, and this stage is also the parameters change stage. As the milling tool enters the CFRP, the axial force continues to rise from 0 N to a maximum of 50 N, and then tends to be stable state. The sixth stage is similar to the second and fourth stages and belongs to the stable milling stage. The axial force in this stage is about 28 N. The seven stage is the stage when the milling tool is about to complete the Al alloy machining. In this stage, the milling axial force is gradually reduced to 0 N. Milling of the Al alloy/CFRP/Al alloy laminations as shown in Fig. 26(b) also goes through the above seven stages. The cutting force of Al alloy and CFRP obtained by hole-making with variable parameters does not change much, but the axial force of CFRP is reduced from the original 40–45 N to 25–30 N.

In summary, it is helpful to improve the quality of the holes by hole-making with variable parameters in laminated materials. This method can not only improve the burr in the gap between the Al alloy and the CFRP laminations, but also improve the tear value of the CFRP. At the same time, it can improve the hole wall morphology of Al alloy and CFRP and reduce the axial force of CFRP.

5 Conclusion

(1) The results of the RSM were analyzed. The pitch and spindle speed have the great influence on the quality of the hole-making. Taking the interlayer burr height of Al alloy and the tear value of CFRP as the judgment standard, the optimal process parameters for Al alloy hole-making are predicted and obtained as follows: the spindle speed is 3000 r/min, the pitch is 0.17 mm and the preload is 380 N and the optimal process parameters for CFRP hole-making are predicted and obtained as follows: the spindle speed is 3700 r/min, the pitch is 0.11 mm and the preload is 430 N.

(2) The cutting forces were analyzed using two sets optimal process parameters. From the experimental results, it can be seen that the machining parameters shown in Fig. 23(a) have relatively small axial force for milling hole, which is suitable for both CFRP and Al alloys. However, the efficiency of this parameters are low, and there is sudden increase in the axial force when the milling tool transitions from CFRP to Al alloy.

(3) Experiments were designed using hole-making processes with variable parameters. Using the optimal process parameters, the feasibility of four different laminated materials are respectively verified. Finally, it is found that the process parameters used as follows: the spindle speed is 3000 r/min and the pitch is 0.17 mm for the Al alloy hole, the spindle speed is 3700 r/min and pitch is 0.11 mm for the CFRP hole

and the preload is 430 N. The parameters are varied at the exit of each material. The burr in the gap between the Al alloy and the CFRP are significantly reduced, and the minimum burr can reach 4.1 μm. The tear value of CFRP is greatly reduced, and the minimum tear is 0.07 mm, which is much smaller than the 2.54 mm required by the process parameters. The axial force of CFRP is reduced from the original 40–45 N to 25–30 N, which is 70% of the hole-making with constant parameters. The axial force of the Al alloy hole-making is 83% of the constant parameters milling hole. The micro-lifting method effectively reduces the sudden change of the axial force between interlayers.

Declarations

Funding This paper was funded by the Natural Science Foundation of Liaoning Province Grant (no.2019-ZD-0029) and the University of Science and Technology Liaoning Talent Project Grants (no.601011507-32).

Code availability Not applicable.

Ethics approval Not applicable.

Consent to participate Not applicable.

Consent for publication Not applicable.

Competing interests The authors declare no competing interests.

References

1. Wang HJ (2016) Investigation on generation mechanism and control strategy of defect in drilling of resin-based composite materials. Shangdong University. https://doi.org/10.76 66/d.Y3033849
2. Wang L, Zhang L, Tian W, Liao WH, Hu J (2017) Control strategy of delamination in drilling carbon Fiber reinforced composi-tes. Aeronautical Science & Technology 28(2):69-73. https://doi.org/10.19452/j.issn 1007-5453.2017.02.069
3. Li WP (2020) Investigation on hole making process and connection performance of CFRP/aluminum alloy laminated compo-nents. Dalian University of Technology
4. Dong ZG, Zhang B, Kang RK, Yang GL, BaoY (2020) A method for restraining axial force in process of helical Milling of CFRP. Aeronautical Manufacturing Technology 63(17):14-20. https://doi.org/10.16080/j.issn 1671-833x.2020.17.014
5. Fang CP, Zhao JZ, Ye ZM, Gou AR Ling L (2020) Progress in helical milling holes for carbon fiber reinforced polymer. Composite Science and Engineering 11: 123-128. https: //doi.org/10.3969/j.issn.1003-0999.2020.11. 020
6. Jiang XY (2021) Study on fatigue performance of aluminum alloy components with helical Milling hole. Dalian University of Technology

7. Editorial committee of china aviation materials manual (2013) China Aviation Materials Manual Volume 3 Aluminum alloy magnesium alloy. Beijing: Tsinghua University Press
8. Guo F, Wang WH, Li ZY, Zhao YP, Xu B (2019) Research on precision hole-making control technology for aerospace laminated materials. China Plant Engineering 22:112-113.https://doi.org/10.3969/j.issn.1671-0711. 2019.22.065
9. Yu HF, Xue HF (2017) Prediction of dynamic thrust Force in drilling of CFRP /aluminum-alloy stacks. Mechanical Science and Techn-ology for Aerospace Engineering 36(1): 68-73. https://doi.org/10.13433/j.cnki. 1003-8728.2017.0110
10. Wang H, Hu J, Sun X (2015) Experimental research on drilling process of carbon fiber reinforced plastic and aluminum alloy stacks. Tool Engineering 49(11): 63-67. https://doi.org/10.16567/j.cnki.1000-7008.2015.11.035
11. Yu XJ, Cao ZQ, Jing HY, Gong YH (2011) Investigation of drilling process for carbon fiber reinforced plastic (CFRP) and titanium sandwich structure. 3:95-97. https://doi.org/1 0.3969/j.issn.1671-833X.2011.03.018
12. Liang J (2013) The formation and effect of interlayer gap in dry drilling of stacked metal materials. International Journal of Advanced Manufacturing Technology 69:1263–1272. https://doi.org/10.1007/s00170-013-5112-9
13. Li Y, Hu YX, Yao ZQ (2014) Experimental investigation of the effect of clamping force on the inter-layer drilling burr of stacked aluminum alloy sheets. Modular Machine Tool Automatic Manufacturing Techni-que 2:110-113. https://doi.org/10.13462/j.cnki.mmtamt.2014.02.029
14. Luo YG, Yuan XM, Zhang Y, Han X, Huang MC (2019) Research on precision hole making process for laminated materials of aircraft. Manufacturing Technology & Machine Tool 9: 122-126. https://doi.org/10.19287/j.cnki.1005-2402.2019.09.026
15. Wei XW, Tian W, Qiu YP, Zhang L, Liao WH (2020) Influence of variable parameters on aperture accuracy of drilling CFRP and aluminum alloy stacks. Machine Building & Automation 1:40-43. https://doi.org/10.19344/j.cnki.issn1671-5276.2020.01.012
16. Zitoune R, Krishnaraj V, Collombet F (2010) Study of drilling of composite material and aluminium stack. Composite Structures 92: 1246-1255https://doi.org/10.1016/j.compstruct.2009.10.010
17. Li C (2019) Research on the technology of lamination of carbon fiber composites and titanium alloys. Telecom World 8:370-371.
18. Gao HZhang XL (2011) Drilling of composite and titanium stacks with alternating machining parameters by PCD drill. International Journal of Machining and Machinability of Materials. 10(4) : 280-292https://doi.org/10.1504/IJMMM.2011.043087
19. Wang GD, Zhou L, Zhong Q, Li N, Xiong XH (2017) Technical investigation on drilling of CFRP /aluminum Stack. Science Technology and Engineering 17(6): 152-157. https://doi.org/10.3969/j.issn.1671-1815.2017.06.027
20. Sun X, Tian W, Liu Z, Li DP (2014) Research on axial force of carbon fiber composites/aluminum alloy laminated hole making. Machinery 52(6):68-70. https://doi.org/10.3969/j.issn.1000-

4998.2014.06.020

21. Wang ZG, Yu SR (2017) The experiment research on drilling of CFRP /titanium alloy stack with varying parameters. Machine Design and Research 30(1): 114-117,126. https://doi.org/10.13952/j.cnki.jofmdr.2017.0025
22. Wei XW (2019) Research on drilling aircraft laminated materials with variable parameters. Nanjing University of Aeronautics and Astronautics
23. Wang SP, Liang J, Cui ST, Zhang ZQ (2022) Analysis of burr morphology of CFRP /Al laminated material in variable feed drilling. Modular Machine Tool Automatic Manufacturing Technique 2:95-98. https://doi.org/10.13462/j.cnki.mmtamt.2022.02.022
24. Ozturk OM, Kilic ZM, Altintas Y (2018) Mechanics and dynamics of orbital drilling operations. International Journal of Machine Tools and Manufacture 129:37-47. https://doi.org/10.1016/j.ijmachtools.2018.03.001
25. Dutra Pereira RB, Brandao LC, De Paiva AP, Ferreira JR, Davim J. Paulo (2017) A review of helical milling process. International Journal of Machine Tools & Manufacture 120:27-48. https://doi.org/10.1016/j.ijmachtools.2017.05.002
26. Durante M, Boccarusso L, De Fazio D, Langella A (2019) Circular cutting strategy for drilling of carbon fiber-reinforced plastics (CFRPs). Materials and Manufactur-ing Processes 34 (5):554-566. https://doi.org/10.1080/10426914.2019.1566615
27. Li JP, Jiao AY, Chen XM (2021) Study on hole making process of thick-section CFRP. International Journal of Advanced Manu-facturing Technology. 117:3369-3378.https://doi.org/10.1007/s00170-021-07929-z
28. Ni WY (2007) Orbital drilling of aerospace materials. Aerospace Technology Confer-ence & Exposition. https://doi.org/10.4271/2007-01-3814
29. Shan YC (2014) Fundamental research on the helical milling process of holes for aero laminated structure materials. Nanjing University of Aeronautics and Astronautics
30. Wang B, Gao H, Cao B, Zhuang Y, Zhao Z (2014) Mechanism of damage generation during drilling of carbon/epoxy compo-sites and titanium alloy stacks. Proceed-ings of the Institution of Mechanical Engineers, Part B: Journal of Engineering Manufacture 228(7):698–706. https://doi.org/10.1177/0954405413508117
31. Sun L, Gao H, Wang B, Bao YJ, Ma SY (2020) Mechanism of reduction of damage during helical milling of titanium/CFRP/aluminium stacks. International Journal of Advanced Manufacturing Technology. 107:11-12. https://doi.org/10.1007/s00170-020-05177-1
32. Huang BT, Luo HQ, Pu JW, Gao YF (2020) Experimental research on variable param-eters of helical milling hole for CFRP/ titanium alloy stacks. Aeronautical Science & Technology 31(9): 65-71. https://doi.org/10.19452/j.issn1007-5453.2020.09.011
33. Fang XE (2019) Research on the hole-making quality of CFRP/Ti alloy laminated materials during a new method of gyro milling process. Nanchang Hangkong University

34. Li Y, Hu YX, Yao ZQ (2014) Experimental investigation of the effect of clamping force on the inter-layer drilling burr of stacked aluminum alloy sheets. Modular Machine Tool & Automatic Manufacturing Technique 2: 110-113. https://doi.org/10.13462/j.cnki.mmtamt.2014.02.029
35. Wang H, Sun X, Hu J (2016) Experimental research on interlayer burrs based on lamination materials under different pressing conditions. Machinery 54(1):51-53. https://doi.org/10.3969/j.issn.1000-4998.2016.01.018
36. Zhang W, Wei G, Xiao XK (2013) Constitutive Relation and Fracture Criterion of 2A12 Aluminum Alloy. Acta Armamentarii 34(3):276-282

Figures

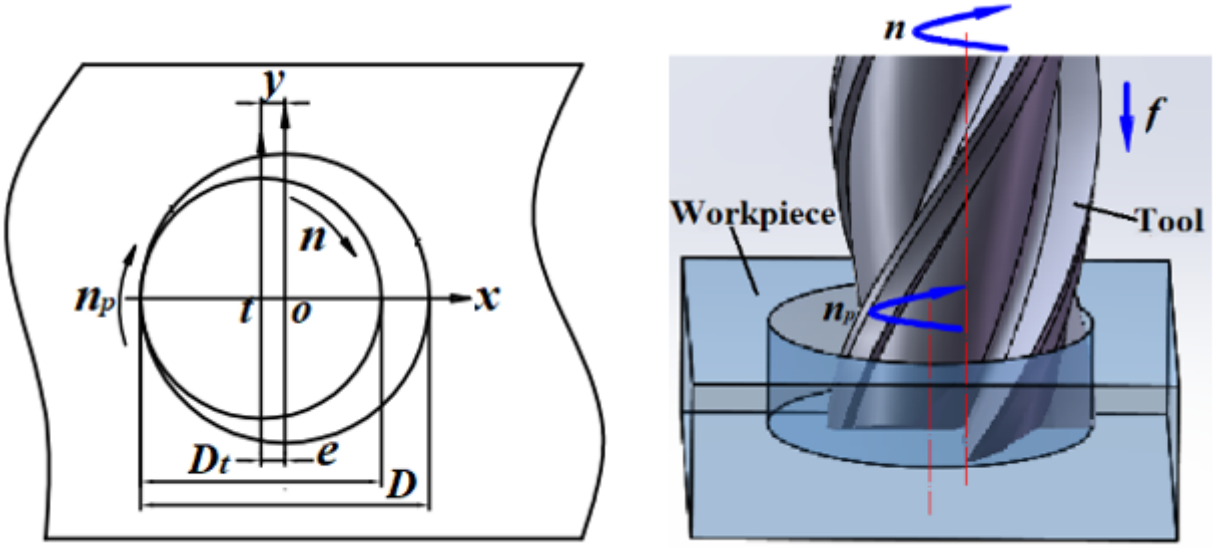

Figure 1

Hole-making schematic diagram

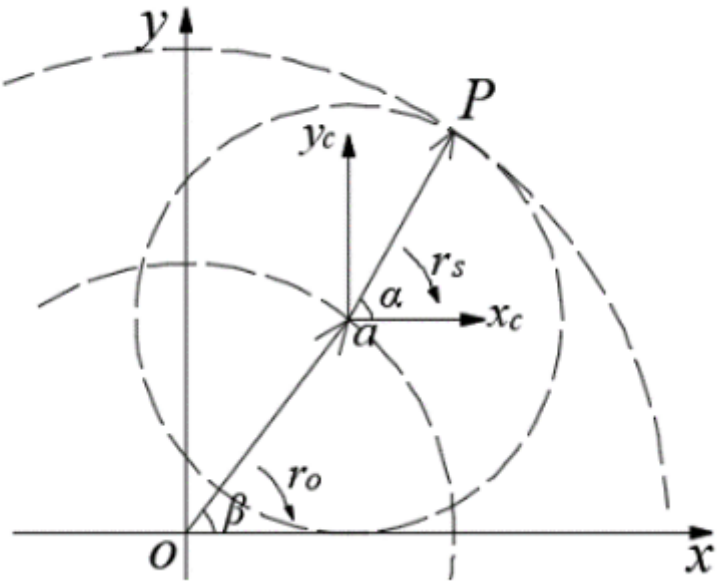

Figure 2

Angle relationship during helical milling

Figure 3

3D trajectory of tool nose

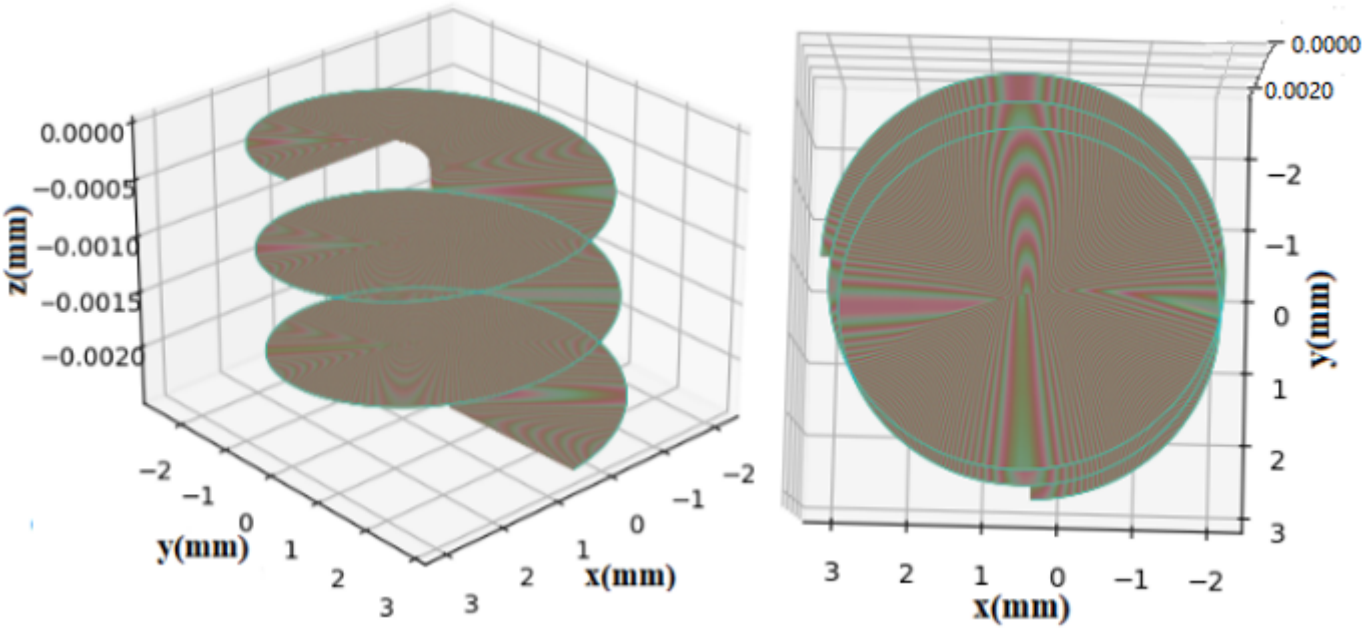

Figure 4

3D trajectory of end edge

Figure 5

3D trajectory of side edge

Figure 6

Al alloy and CFRP

Figure 7

Analysis of burr height of Al alloy. **a** Residual normal diagram. **b** Correspondence between residual and equation prediction value

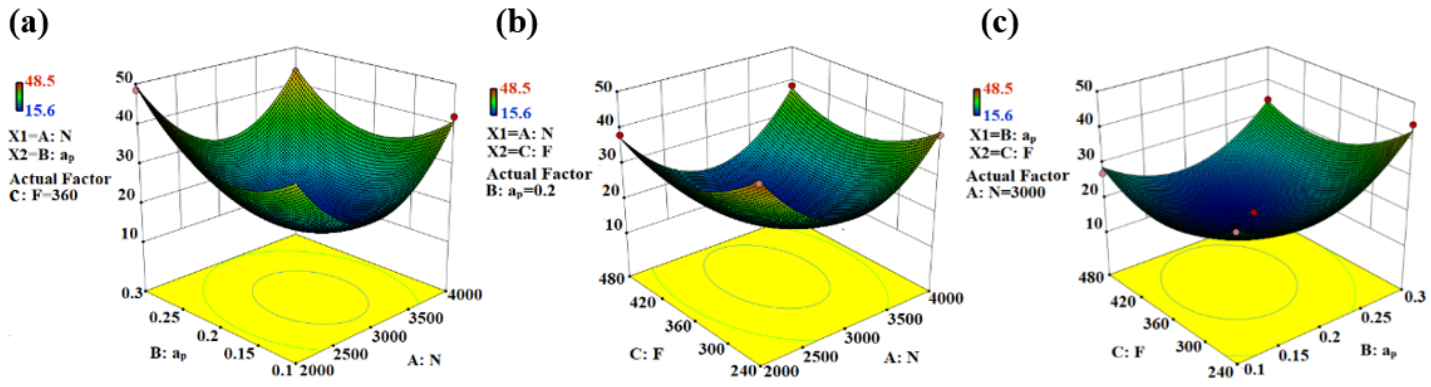

Figure 8

The influence of the interaction of various process parameters on the exit burr height. **a** Spindle speed and pitch. **b** Spindle speed and preload. **c** Pitch and preload

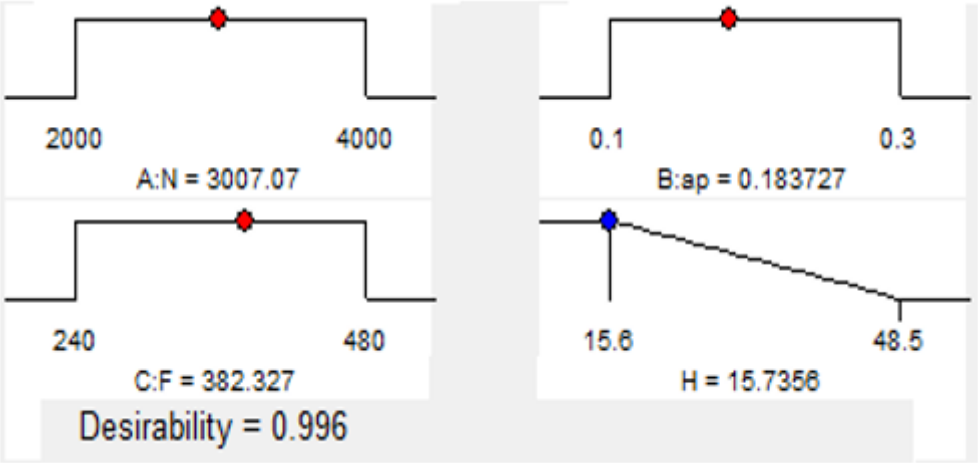

Figure 9

The optimal process parameters

Figure 10

Analysis of tear value of CFRP. **a** Residual normal diagram. **b** Correspondence between residual and equation prediction value

Figure 11

The influence of the interaction of various process parameters on the exit tear value. **a** Spindle speed and pitch. **b** Spindle speed and preload. **c** Pitch and preload

Figure 12

The optimal process parameters

Figure 13

Analysis of tear value of CFRP. **a** Residual normal diagram. **b** Correspondence between residual and equation prediction value

Figure 14

The influence of the interaction of various process parameters on the exit tear value. **a** Spindle speed and pitch. **b** Spindle speed and preload. **c** Pitch and preload

Figure 15

The optimal process parameters

Figure 16

Analysis of tear value of Al alloy. **a** Residual normal diagram. **b** Correspondence between residual and equation prediction value

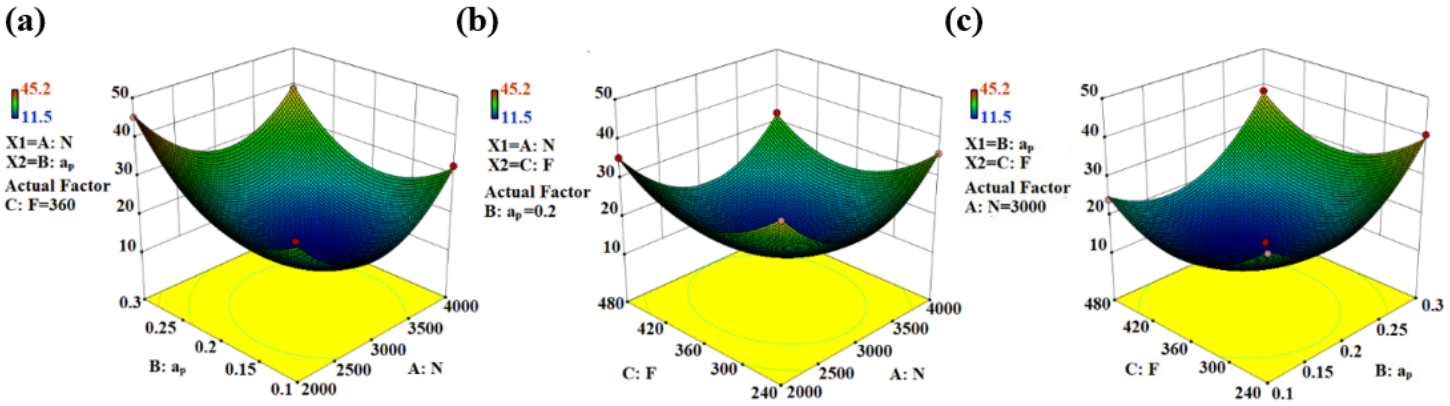

Figure 17

Influence of interaction of process parameters on burr height. **a** Spindle speed and pitch. **b** Spindle speed and preload. **c** Pitch and preload

Figure 18

The optimal process parameters

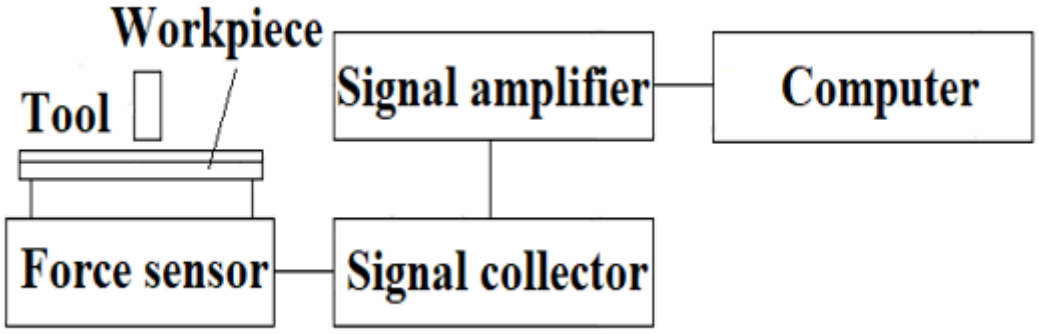

Figure 19

Data acquisition schematic diagram

Figure 20

Milling force comparison of CFRP/Al alloy laminated materials. **a** The optimal parameters combination of CFRP. **b** The optimal parameters combination of Al alloy

Figure 21

Defects of the entrance and exit of the hole

Figure 22

The burr 3D morphology of entrance and exit of the hole. **a** CFRP/ Al alloy. **b** Al alloy /CFRP. **c** CFRP/ Al alloy /CFRP. **d** Al alloy /CFRP/ Al alloy. **e** Al alloy/ CFRP/ Al alloy

Figure 23

Morphology of hole wall of CFRP. **a** CFRP/ Al alloy. **b** Al alloy /CFRP. **c** CFRP/ Al alloy /CFRP. **d** CFRP/ Al alloy/ CFRP. **e** Al alloy/ CFRP/ Al alloy

Figure 24

Morphology of hole wall of Al alloy. a CFRP/ Al alloy. b Al alloy /CFRP. c RP/ Al alloy/ CFRP. e Al alloy/ CFRP/ Al alloy

Figure 25

Milling force comparison laminated materials. **a** CFRP/ Al alloy. **b** Al alloy /CFRP

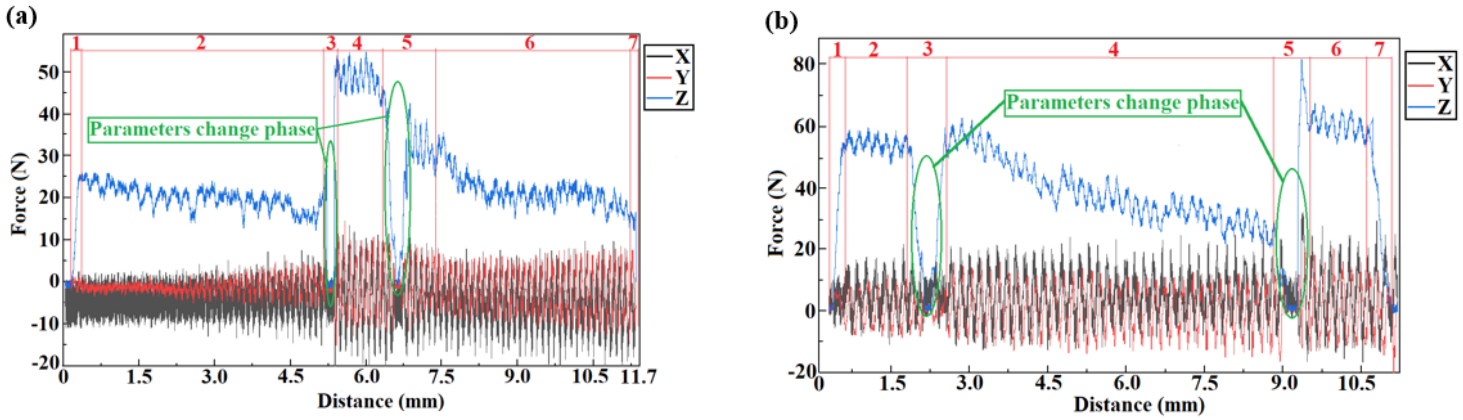

Figure 26

Milling force comparison of laminated materials. **a** CFRP/Al alloy/ CFRP. **b** Al alloy/CFRP/ Al alloy